JOURNAL OF SPACECRAFT AND ROCKETS
Vol. 29, No. 5, September–October 1992

Payload Vehicle Aerodynamic Re-Entry Analysis

Donald Tong*
Boeing Defense & Space Group, Seattle, Washington 98124

This paper provides an approach to analyze the dynamic behavior of a cone-cylinder payload vehicle during re-entry to ensure successful deployment of the parachute system and payload recovery. Estimates of the static aerodynamic forces and moments, dynamic damping moments, and high angle-of-attack asymmetric forces are made. A dynamics simulation is then performed based on these estimates to obtain the vehicle attitude and rate histories during re-entry. The vehicle is stable in pitch, and the roll behavior can be manipulated. However, controlling and predicting flat spin accurately have been found to be difficult.

Nomenclature

A = reference area, $\pi d^2/4$
C_A = axial force coefficient
C_d = two-dimensional cylinder drag coefficient
C_l = rolling moment coefficient, $L/(q_\infty Ad)$
C_{lp} = roll damping coefficient, $\partial C_l/\partial(pd/2V_\infty)$
C_m = pitching moment coefficient, $M/(q_\infty Ad)$
C_{mq} = pitch damping coefficient, $\partial C_m/\partial(qd/2V_\infty)$
C_N = normal force coefficient
C_n = yawing moment coefficient, $N/(q_\infty Ad)$
C_{nr} = yaw damping coefficient, $\partial C_n/\partial(rd/2V_\infty)$
C_s = two dimensional side force coefficient
d = body cylinder diameter
dL = local body diameter
Ii = moment of inertia about the body axis i, $i = x$, y, or z
L = body moment about the roll axis x
Lv = vehicle body length
M = body moment about the pitch axis y
N = body moment about the yaw axis z
p = body roll rate
q = body pitch rate
q_∞ = freestream dynamic pressure
Re = Reynolds number, $\rho_\infty V_\infty\, dL/\mu$
r = body yaw rate
V_∞ = freestream velocity
X = distance from nose in the axial direction
x_{cg} = distance from nose to center of gravity
α = angle of attack
η = correction for finite cylinder length and Mach number
θ = Euler angle (pitch)
μ = atmospheric viscosity
ρ_∞ = atmospheric density
ϕ = Euler angle (roll)
φ = roll angle measured from the downward axis in the vehicle yz plane to the z axis
ψ = Euler angle (yaw)
ω = body rate matrix

Received March 4, 1991; presented as Paper 91-0865 at the AIAA 11th Aerodynamic Decelerator Systems Technology Conference, San Diego, CA, April 9–11, 1991; revision received July 14, 1991; accepted for publication July 31, 1991.

*Specialist Engineer, P.O. Box 3999. Member AIAA.

Introduction

WHEN payload vehicles are boosted into space by sounding rockets to carry out experiments in the exoatmospheric environment, very often these vehicles and the expensive instruments they carry are to be recovered for future flights. The purpose of this analysis is to understand and refine the dynamic behavior of a cone-cylinder payload vehicle to ensure that the vehicle and the instruments it carries will survive re-entry and to provide attitude and rate data at parachute deployment for designing a parachute recovery system. Modeling vehicle motion during re-entry requires estimates of the static aerodynamic forces and moments, the dynamic damping moments, and the asymmetric forces during a flat spin. A simulation then uses these inputs and generates the vehicle dynamic motion prior to deployment of the parachute.

To eliminate concentration of surface aerodynamic heating, vehicle spin-up about the longitudinal axis is instituted before re-entry. However, flight data have shown that payload vehicle spinning stops when dynamic pressure starts to build up during re-entry. This analysis includes the study of a simple aerodynamic device useful in sustaining vehicle axial rotation through the maximum dynamic pressure region.

Low vehicle descent rate at parachute deployment is required to avoid using heavier parachute lines, deploying a larger drogue parachute to slow down and stabilize the payload, using multiple parachute staging, etc., all of which contribute to a heavier recovery system. To minimize descent speed, the vehicle center of gravity is designed to coincide with the longitudinal aerodynamic center of pressure at the desired trim angle of attack of approximately 90 deg. Base-down re-entry ($\alpha \approx 108$ deg) is to be avoided because there is a greater chance of the parachute entangling with the vehicle at deployment. Flat re-entry also minimizes the undesirable yawing moment resulting from vortex shedding, which has the largest magnitude at angles of attack between 30 and 60 deg. Yawing moment exists even at $\alpha \approx 90$ deg when the local Reynolds number is in the critical region and a laminar separation bubble occurs on just one side of the vehicle. The difference in the flow separation patterns on the two sides of the body causes the vehicle to descend in a propellerlike motion (flat spin) during the subsonic portion of re-entry.

The parachute recovery system (a cylindrical section) is attached to the base of the vehicle. At about 15 kft in altitude, a pressure sensing device will activate the system and a pilot parachute will be ejected out of the recovery system base plate pulling out the drogue parachute, and the drogue parachute will in turn deploy the main parachute. To design the parachute staging and reefing and to estimate the parachute line loads, a parachute deployment dynamic analysis will be required. The results from this paper will provide the initial conditions required to conduct this analysis.

Analysis

Vehicle Configuration and Re-Entry Trajectory

The following vehicle mass characteristics and initial conditions are used to predict the aerodynamics and the re-entry trajectory:

Mass	915 kg
Ix	115 kg m^2
$Iy = Iz$	868 kg m^2
Velocity at 91 km	1.95 km/s

Figure 1 shows the configuration on the payload vehicle. A nominal point-mass re-entry trajectory is established based on the vehicle weight, the re-entry initial state vector, and the aerodynamic drag of the vehicle at the predicted trim angle of attack ($\alpha \sim 90$ deg). The results, shown in Fig. 2, provide histories of dynamic pressure, velocity, and altitude that are used in the re-entry dynamic analysis integration scheme to obtain vehicle attitude and rate.

Derivation of Pitch Static and Dynamic Aerodynamics

Static aerodynamic coefficients for the cone-cylinder vehicle are obtained based on the empirical slender-body potential and viscous crossflow methods[1,2] neglecting any surface protuberances. Selected data points have been verified by two independent wind-tunnel tests. Results from the calculations are shown in Figs. 3–5. Figure 6 also shows the c.g. location required for the re-entry trim angle of 90 deg.

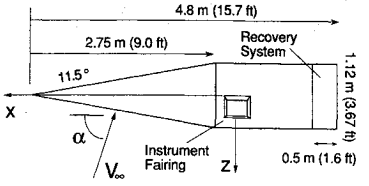

Fig. 1 Vehicle geometry.

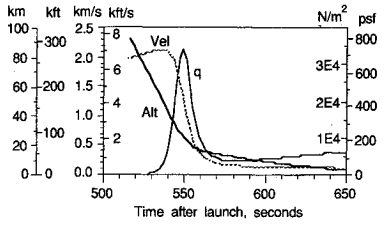

Fig. 2 Dynamic pressure, velocity, and altitude histories.

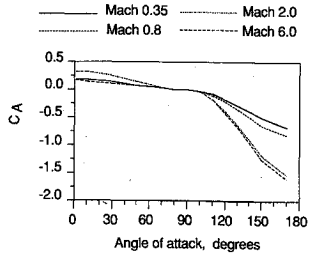

Fig. 3 Axial force coefficient.

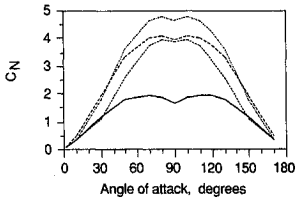

Fig. 4 Normal force coefficient.

At 90-deg angle of attack, the pitch damping coefficient C_{mq} can be derived by integrating the local forces on the body. The local forces vary with the local velocity along the body. The local velocity, in turn, depends on the pitch rate q. Figure 7 shows the geometry needed to derive C_{mq} at α near 90 deg.

$$\text{Moment}\,|_{\alpha=90\text{ deg}} = \int [\text{local force } x]\, dx$$

$$= \int [C_d(0.5\rho_\infty V_L^2)\, dL\, (x_{cg} - x)]\, dx \qquad (1a)$$

$$C_m\,|_{\alpha=90\text{ deg}} = \int [C_d(0.5\rho_\infty V_L^2)\, dL\, (x_{cg} - x)]\, dx$$

$$/(Ad0.5\rho_\infty V_\infty^2) \qquad (1b)$$

with

$$V_L = V_\infty - q(x_{cg} - x)$$

$$V_L^2 \approx V_\infty^2 - 2V_\infty q(x_{cg} - x)$$

$$C_m\,|_{\alpha=90\text{ deg}} \approx \int [C_d\, dL\, (x_{cg} - x)]\, dx/(Ad)$$

$$-2\int [C_d q(x_{cg} - x)^2\, dL]\, dx/(AdV_\infty) \qquad (1c)$$

The first term of Eq. (1c) is the moment due to the static force and the second term, being a function of q, is the dynamic damping term. The damping coefficient, as indicated in Eq. (2), is derived by differentiating this term with respect to q and is nondimensionalized by being divided by $(d/2V_\infty)$.

$$\therefore C_{mq}\,|_{\alpha=90\text{ deg}} \approx \partial C_m\,|_{\alpha=90\text{ deg}}/\partial(qd/2V_\infty)$$

$$\approx -4\int [Cd(x_{cg} - x)^2\, dL]\, dx/(Ad^2) \qquad (2)$$

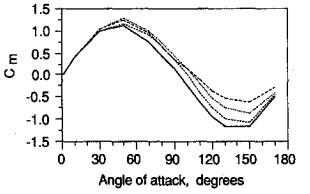

Fig. 5 Pitching moment coefficient.

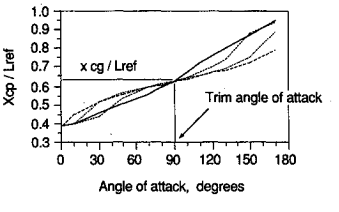

Fig. 6 Center of pressure.

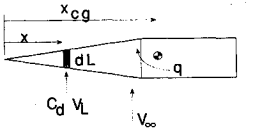

Fig. 7 Schematic description of coordinate system.

C_{mq} near $\alpha = 0$ and 180 deg in the subsonic region is estimated by using the modified slender-body theory and in the supersonic region the gamma corrected Newtonian theory.[3] As a simplification, the estimations are then merged to complete the derivation, ignoring the nonlinear effect due to vortex shedding at angles of attack between 30–60 deg. Since the vehicle spends most of its trajectory at $\alpha = 90$ deg, this simplification will not have a significant effect on the final results. Figure 8 shows the derived C_{mq} as a function of angle of attack and Mach number.

Yawing Moment Modeling

At angle of attack in the region of 25–70 deg and crossflow Mach less than 1, vortices develop asymmetrically and detach down the length of the slender body. As a result, asymmetric side force and a yawing moment of significant magnitude can be developed and are usually undesirable. However, at angles of attack near 90 deg (vehicle longitudinal axis perpendicular to velocity), this effect weakens and is dominated by a different side force phenomenon resulting from the difference in boundary-layer separation on the two sides of the body. When the local flowfield is in the critical Reynolds number region, minute asymmetries (from surface roughness or protuberances, for example) will sometimes cause a turbulent reattachment after a laminar separation on just one side of the body creating a separation bubble.[4,5] The flow is unstable and it is difficult to predict when and at which side of the body it would occur. The resulting yawing moment causes the vehicle to enter into a flat spin. Figure 9 illustrates the asymmetrical flowfield.

This effect diminishes in the supersonic region. Figure 10 describes the forces acting on the vehicle due to the asymmetric flowfield. The phenomenon is assumed to occur consistently on the same side, and the worst-case yawing moment model can be developed[6] by integrating along the body length the following equation (α near 90 deg):

$$C_n = \int [(C_s \cos\gamma - C_d \sin\gamma |x - x_{cg}| dL/(Ad)]\, dx \sin\alpha \quad (3)$$

where

$$\tan\gamma = |x - x_{cg}| r / V_\infty$$

The values of C_s and C_d, functions of local Reynolds number, are derived from experimental data.[6] This model compares well with wind-tunnel results at low Reynolds number and low velocity flows according to the reference literature. To thoroughly understand this phenomenon for the class of vehicle in this analysis, flight testing and/or wind-tunnel testing near flight flow conditions are recommended.

Yaw damping coefficient $C_{nr} \approx 0$ is assumed due mainly to the lack of an accurate method to estimate its value. This assumption will contribute to the uncertainty of the flat spin rate calculation.

Rolling Moment Modeling

There are two main contributors to the rolling moment at α near 90 deg. The dominant one is due to a radially offset center of gravity. The center of pressure is assumed to be at the vehicle center. Surface protuberances also produce a rolling moment near $\alpha = 90$ deg. Figures 11 illustrate the two sources of rolling moment. Equation (4) describes the total rolling moment as a function of α:

$$C_l = (C_{l\,\text{cg offset}} + C_{l\,\text{fairing}})|_{\alpha=90\,\text{deg}} \sin^2\alpha \quad (4)$$

C_l due to c.g. offset is calculated as indicated in Eq. (5). C_l induced by surface protuberances ($C_{l\,\text{fairing}}$) is evaluated as a function of roll angle φ with a computational fluid dynamics code.[7,8] Dimensions and the estimated rolling moment of the instrument fairing at Mach 5 are shown in Figs. 12 and 13, respectively.

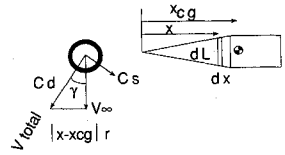

Fig. 10 Schematic description of force vectors and flowfields.

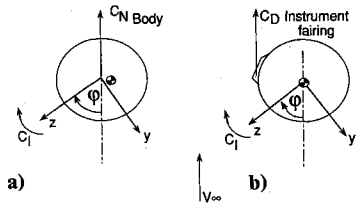

Fig. 11 Rolling moment at $\alpha = 90$ deg; a) c.g. offset; b) protuberances.

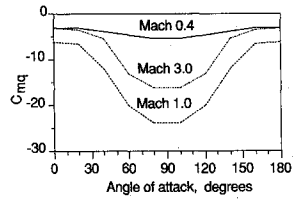

Fig. 8 Pitch damping coefficient.

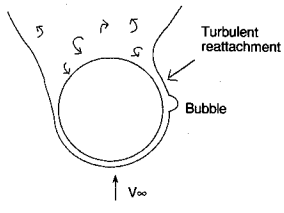

Fig. 9 Asymmetrical flowfield around a circular cylinder in the critical *Re* region.

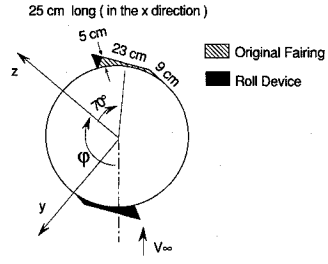

Fig. 12 Dimensions of the instrument fairing and roll device.

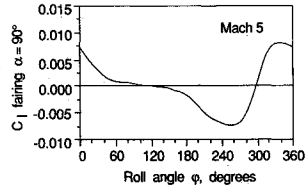

Fig. 13 Rolling moment induced by fairing.

$$C_{l\,\text{cg offset}}|_{\alpha=90\text{ deg}} = C_N|_{\alpha=90\text{ deg}} \sqrt{\Delta y^2 + \Delta z^2}\,\sin\xi/d \qquad (5)$$

where Δy is the c.g. offset in the vehicle body y axis, Δz is the c.g. offset in the vehicle body z axis, and $\xi = \tan^{-1}(\Delta y/\Delta z) - \varphi$. The c.g. offset has the effect of stabilizing the vehicle in roll ($C_l = 0$) with the center of pressure (assumed to be at the center of the cylinder) trailing the c.g. Surface protuberances have the same effect, stabilizing the vehicle with the fairing in the wake. Pre-re-entry spin-up is intended for re-entry aerodynamic heating distribution. However, simulations (verified by flight data) have shown that the roll rate decreases to zero when the dynamic pressure starts to build up. Both the c.g. offset and the surface protuberance contribute to stopping the spin.

An accurate estimate of the roll damping coefficent C_{lp} is difficult to obtain by analysis. Roll characteristics derived from flight acceleration data indicate that a reasonable estimate for C_{lp} is -10.

Aerodynamic Roll Device Modeling

Roll rate can be sustained by slightly modifying the existing fairing and adding a dummy fairing on the opposite side. The configuration and the resulting moment at Mach 5 are illustrated in Figs. 12 and 14, respectively.

A vehicle with a c.g. offset of 0.36 cm and an initial spin rate of 90 deg/s stops spinning before maximum dynamic pressure. With the aerodynamic device, simulations show that spinning can be extended into the maximum dynamic pressure region. This is discussed in the following section.

Payload Vehicle Re-Entry Dynamics

To analyze the payload vehicle attitude during re-entry, the angular momentum equation $\mathbf{Moment} = \mathrm{d}(I\omega)/\mathrm{d}t$ is most useful when the elements are expressed in the aeroballistic axis system,[9] which does not share body roll rate but does share all other body angular rates. The aeroballistic system is illustrated in Fig. 15. Equation (6) is obtained by carrying out the differentiation:

$$\mathbf{Moment}_{\text{body}} = I\dot{\omega}_{\text{body}} + \Omega_{a/i}\, x(I\omega_{\text{body}}) \qquad (6)$$

Since the angular rate of the aeroballistic system with respect to the inertial system does not involved p ($p = 0$ in the skew-symmetric matrix $\Omega_{a/i}$), the equation becomes,

$$\begin{bmatrix} L \\ M \\ N \end{bmatrix} = \begin{bmatrix} Ix & \mathrm{d}p/\mathrm{d}t \\ Iy & \mathrm{d}q/\mathrm{d}t \\ Iy & \mathrm{d}r/\mathrm{d}t \end{bmatrix} + \begin{bmatrix} 0 & -r & q \\ r & 0 & 0 \\ -q & 0 & 0 \end{bmatrix} \begin{bmatrix} Ix & 0 & 0 \\ 0 & Iy & 0 \\ 0 & 0 & Iy \end{bmatrix} \begin{bmatrix} p \\ q \\ r \end{bmatrix} \qquad (7)$$

Euler angles ϕ, θ, and ψ are obtained from the 3-2-1 axis rotation defining the rotation from the inertial frame to the aeroballistic system. The relationships of the Euler angles and the body rates are defined by Eqs. (8a–c):

$$\mathrm{d}\phi/\mathrm{d}t = q\sin\phi\tan\theta + r\cos\phi\tan\theta \qquad (8a)$$

$$\mathrm{d}\theta/\mathrm{d}t = q\cos\phi - r\sin\theta \qquad (8b)$$

$$\mathrm{d}\psi/\mathrm{d}t = q\sin\phi\sec\theta + r\cos\phi\sec\theta \qquad (8c)$$

Rewriting the angular momentum equations, Eq. (7),

$$\mathrm{d}p/\mathrm{d}t = L/Ix \qquad (9a)$$

$$\mathrm{d}q/\mathrm{d}t = (M - rpIx)/Iy \qquad (9b)$$

$$\mathrm{d}r/\mathrm{d}t = (N + qpIx)/Iy \qquad (9c)$$

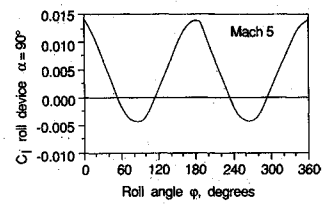

Fig. 14 Rolling moment induced by roll device.

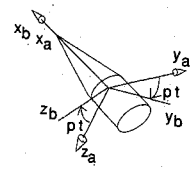

Fig. 15 Aeroballistic and body axes.

and defining the body roll angle φ as

$$\mathrm{d}\varphi/\mathrm{d}t = p \qquad (10)$$

the seven differential equations are then solved simultaneously and integrated through re-entry using the Runge-Kutta scheme. Nominal trajectory data (velocity, dynamic pressure, etc.) are provided to the simulation to scale the aerodynamic coefficients, obtaining the aerodynamic moments L, M, and N:

$$L = C_l(q_\infty Ad) + C_{lp}(q_\infty Ad^2)p/(2V_\infty) \qquad (11a)$$

$$M = C_m(q_\infty Ad) + C_{mq}(q_\infty Ad^2)q/(2V_\infty) \qquad (11b)$$

$$N = C_n(q_\infty Ad) + C_{nr}(q_\infty Ad^2)r/(2V_\infty) \qquad (11c)$$

The three angles, φ, θ, and ψ, completely define the vehicle attitude and are outputs of the simulation.

Initial conditions are

$$\phi_i = 0, \qquad \mathrm{d}\phi/\mathrm{d}t_i = 90 \text{ deg/s}$$

$$\phi_i = \alpha_i - 90 \text{ deg} = -20 \text{ deg}, \qquad \mathrm{d}\theta/\mathrm{d}t_i = 0$$

$$\psi_i = 0, \qquad \mathrm{d}\psi/\mathrm{d}t_i = 0$$

$$\varphi_i = 0$$

Figure 16 shows the simulated attitude rates of the vehicle throughout the entire re-entry phase. The initial pitch deviation from trim is arbitrarily assumed to be -20 deg. The pitch motion damps out quickly after the start of atmospheric re-entry. The restoring motion in pitch creates a gyroscopic effect, generating a slow motion in yaw, since the vehicle is rotating about the longitudinal axis at about 90 deg/s. When the dynamic pressure starts to build up at about 540 s, this axial rotation stops abruptly and turns into roll oscillations and finally damps out as it exits the maximum dynamic pressure region. This effect is due to the aerodynamic moments induced by the instrument fairing and the radial offset in center of gravity. Installing a roll device will extend the rotation in the maximum dynamic pressure region. Figure 17 shows the effectiveness of the aerodynamic roll device described in the previous section as a function of center of gravity offset. Figure 18 indicates that a minimum initial spin rate of 90 deg/s is required to obtain the longest spin time. In the subsonic region (time > 565 s), the vehicle enters a flat spin (in yaw), and if the flow asymmetry is assumed to last throughout this region (worst-case situation), the vehicle yaw rate will build up to about 60 deg/s at parachute deployment (640 s).

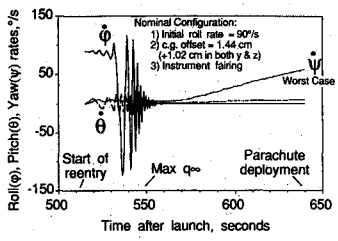

Fig. 16 Vehicle roll, pitch, and yaw attitude rates.

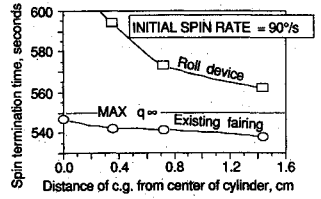

Fig. 17 Axial spin extension.

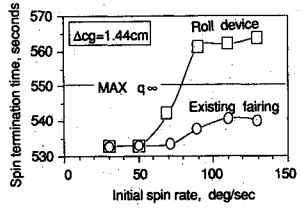

Fig. 18 Effect of initial spin rate.

Conclusions

At parachute deployment, the vehicle has a very stable pitch motion. The worst-case yaw rate (flat spin) is about 60 deg/s and the vehicle is not spinning about the longitudinal axis. Placing the c.g. close to the radial center of the cylinder lowers the maximum spin rate during maximum dynamic pressure. However, a c.g. location within 1.0 cm of the center may be difficult to obtain. Axial spinnning through maximum dynamic pressure is desirable for the distribution of aerodynamic heating. This can't be achieved with the nominal configuration. However, spinning can be sustained through the maximum dynamic pressure region if a roll device similar to the one examined in the study is installed. The maximum spin rate during maximum dynamic pressure and spin termination time can be refined by modifying the shape of the roll device. The roll and yaw dynamic damping terms are difficult to obtain and the assumptions used in the analysis may contribute to the uncertainty of the roll oscillation and flat spin rate calculations. Finally, estimates of the vehicle dynamics at parachute deployment are defined and can be provided as initial conditions to a parachute deployment dynamic analysis required for designing a successful payload recovery system.

References

[1]Jorgensen, L. H., "Prediction of Static Aerodynamic Characteristics for Space-Shuttle-Like and Other Bodies at Angles of Attack from 0° to 180°," NASA TND-6996, Jan. 1973.

[2]Finck, R. D., "USAF Stability and Control DATCOM," Air Force Flight Dynamics Laboratory, Task No. 821901, Wright-Patterson Air Force Base, OH, April 1978.

[3]Ericsson, L. E, and Reding, J. P., "Approximate Slender Vehicle Dynamics At All Speeds," *Proceedings of the 11th Navy Symposium on Aeroballistics,* Aug. 1978, pp. 87–114.

[4]Clarke, A. J., "Normal Force Pitching Moment and Side Force of Forebody-Cylinder Combinations for α up to 90° and Mach Up To 5," Engineering Sciences Data Unit, Royal Aeronautical Society, Item No. 89014, London, Aug. 1989.

[5]Bearman, P. W., "On Vortex Shedding from a Circular Cylinder in the Critical Reynolds Number Regime," *Journal of Fluid Mechanics,* Vol. 37, July 1969, pp. 577–585.

[6]Yoshinaga, T., Tate, A., and Inoue, K., "Approximate Calculation of Aerodynamic Coefficients for Rotating Slender Bodies at 90° Incidence," *Journal of Spacecraft and Rockets,* Vol. 19, No. 1, 1982, pp. 84–86.

[7]Birch, S. F., "Development of an Advanced Navier-Stokes Analysis Capability," AIAA Paper 88-0719, Jan. 1988.

[8]Hoffman, J. J., "Development of an Algorithm for the Three-Dimensional Fully-Coupled Navier-Stokes Equations with Finite Rate Chemistry," AIAA Paper 89-0670, Jan. 1989.

[9]Regan, F. J., *Reentry Vehicle Dynamics,* AIAA, Education Series, New York, 1984, pp. 236–238.

Gerald T. Chrusciel
Associate Editor